Kaon BSM B-parameters using improved staggered fermions from N_{f}=2+1 unquenched QCD

Benjamin J. Choi, Yong-Chull Jang, Chulwoo Jung, Hwancheol Jeong, Jangho Kim, Jongjeong Kim, Sunghee Kim, Weonjong Lee, Jaehoon Leem, Jeonghwan Pak, Sungwoo Park, Stephen R. Sharpe, and Boram Yoon (SWME Collaboration)

Kaon BSM B-parameters using improved staggered fermions from $N_f = 2+1$ unquenched QCD

Benjamin J. Choi,[1] Yong-Chull Jang,[1] Chulwoo Jung,[2, *] Hwancheol Jeong,[1] Jangho Kim,[3] Jongjeong Kim,[1] Sunghee Kim,[1] Weonjong Lee,[1, †] Jaehoon Leem,[1] Jeonghwan Pak,[1] Sungwoo Park,[1] Stephen R. Sharpe,[4, ‡] and Boram Yoon[5]

(SWME Collaboration)

[1] *Lattice Gauge Theory Research Center, FPRD, and CTP,*
Department of Physics and Astronomy, Seoul National University, Seoul 08826, South Korea
[2] *Physics Department, Brookhaven National Laboratory, Upton, NY11973, USA*
[3] *National Institute of Supercomputing and Networking,*
Korea Institute of Science and Technology Information, Daejeon 34141, South Korea
[4] *Physics Department, University of Washington, Seattle, WA 98195-1560, USA*
[5] *Los Alamos National Laboratory, Theoretical Division T-2, MS B283, Los Alamos, NM 87545, USA*
(Dated: December 22, 2015)

We present results for the matrix elements of the additional $\Delta S = 2$ operators that appear in models of physics beyond the Standard Model (BSM), expressed in terms of four BSM B-parameters. Combined with experimental results for ΔM_K and ϵ_K, these constrain the parameters of BSM models. We use improved staggered fermions, with valence HYP-smeared quarks and $N_f = 2+1$ flavors of "asqtad" sea quarks. The configurations have been generated by the MILC collaboration. The matching between lattice and continuum four-fermion operators and bilinears is done perturbatively at one-loop order. We use three lattice spacings for the continuum extrapolation: $a \approx 0.09$, 0.06 and 0.045 fm. Valence light-quark masses range down to $\approx m_s^{\mathrm{phys}}/13$ while the light sea-quark masses range down to $\approx m_s^{\mathrm{phys}}/20$. Compared to our previous published work, we have added four additional lattice ensembles, leading to better controlled extrapolations in the lattice spacing and sea-quark masses. We report final results for two renormalization scales, $\mu = 2$ GeV and 3 GeV, and compare them to those obtained by other collaborations. Agreement is found for two of the four BSM B-parameters (B_2 and B_3^{SUSY}). The other two (B_4 and B_5) differ significantly from those obtained using RI-MOM renormalization as an intermediate scheme, but are in agreement with recent preliminary results obtained by the RBC-UKQCD collaboration using RI-SMOM intermediate schemes.

I. INTRODUCTION

Neutral kaon mixing and the associated indirect CP-violation have long provided an important window into physics at high energy scales. In the Standard Model (SM), for example, the measured CP-violating parameter ϵ_K is sensitive to scales up to the top-quark mass. To determine whether the measured value is consistent with the SM, however, requires knowledge of the hadronic matrix element parametrized by the kaon B-parameter, B_K. Recently, lattice QCD calculations have matured to the point that such matrix elements can be determined from first principles with percent-level accuracy.[1] Specifically, results for B_K from Refs. [2–9] are such that the average has an error of $\sim 1.3\%$ [1]. This is accurate enough to provide strong constraints on SM parameters (see, e.g., Refs. [10, 11]). Ultimately, lattice calculations will also be able to use the $K_L - K_S$ mass difference, ΔM_K, to test the SM [12].

Physics beyond the SM (BSM) will, in general, contribute to flavor changing neutral processes such as kaon mixing. Indeed, unless there is some cancellation akin to the GIM mechanism, rough estimates show that the scale of new physics must be $\gtrsim 10^5$ TeV in order to avoid overly large contributions to ΔM_K and ϵ_K [13]. In fact, many BSM models have partial cancellations such that the scale of new physics is accessible at the Large Hadron Collider (LHC), but often such models are pushing against the constraints from kaon mixing. If evidence for new physics is discovered at the LHC in the coming years, then, in order to sift through the available models, it will be essential to turn the constraints from kaon mixing into precision tools. To do this it is necessary to calculate the hadronic matrix elements of the full basis of $\Delta S = 2$ four-fermion operators that can appear. Illustrations of how these matrix elements constrain BSM models are given in Refs. [14–17].

In the SM, four-fermion operators in the effective $\Delta S = 2$ Hamiltonian are composed of left-handed currents. Generic BSM physics, by contrast, also includes heavy virtual particles coupling to right-handed quarks. Because of this, the single "left-left" $\Delta S = 2$ four-fermion

---

* E-mail: chulwoo@bnl.gov
† E-mail: wlee@snu.ac.kr
‡ E-mail: srsharpe@uw.edu
[1] For a recent review of such quantities and their associated errors, see Ref. [1].

operator is augmented by four additional operators. Our aim in the present work is to provide fully controlled results for the corresponding additional mixing matrix elements.

Calculations of such matrix elements using lattice QCD have a fairly long history. Initial results were obtained starting in the late 1990s in the quenched approximation [18–20]. Then, in 2012, first results with unquenched light quarks were presented by the ETM [13] and RBC-UKQCD collaborations [21]. These calculations used, respectively, twisted-mass and domain-wall lattice fermions. Both performed the matching of lattice and continuum operators using non-perturbative renormalization (NPR) [22] and the RI-MOM scheme. The results for all four BSM B-parameters were consistent between the two calculations.

In 2013, we presented results from a first calculation of the BSM B-parameters using improved staggered fermions and one-loop perturbative matching of lattice and continuum operators [23]. Our results disagreed significantly for two of the four B-parameters with those from Refs. [13, 21]. In 2014, we discovered a minor error in our analysis that changed our results by $\sim 5\%$. We also extended the range of lattice ensembles studied, so that the continuum and chiral extrapolations were better controlled. Preliminary results correcting the analysis and incorporating the new ensembles were presented in Ref. [24]. The discrepancy with Refs. [13, 21] remained at about the 3σ level for two of the B-parameters.

The purpose of the present paper is provide a detailed description of our calculation along with our final results. In fact, these results are very close to the preliminary numbers presented in Ref. [24], but there are many details not provided in either Ref. [23] or [24] that we present here. A further motivation for this work is provided by the recent results from the ETM and RBC-UKQCD collaborations, presented in Refs. [3] and at Lattice 2015 [25, 26], respectively. The former work (which extends the $N_f = 2$ simulations of Ref. [13] to $N_f = 2+1+1$) essentially confirms the earlier results of Ref. [13], and thus continues to disagree with our results. The latter calculation, Ref. [25], presents an investigation of the origin of the discrepancies by repeating their computation with a second lattice spacing and performing the renormalization with various schemes, including RI-SMOM schemes with non-exceptional kinematics [27]. Although the discretization artifacts are found to be larger than previously anticipated, the most important effects come from the renormalization procedure. The preliminary results of RBC-UKQCD with the new SMOM schemes are in approximate agreement with those presented here [26]. Given this complicated and confusing situation, it is important to have a clear description of the details of all the calculations.

Our work relies on several auxiliary theoretical calculations. For the chiral extrapolations we need results from SU(2) staggered chiral perturbation theory (SChPT), and these are provided in Ref. [28]. We also need to know how to set up the calculation using staggered fermions (i.e. dealing with the extra valence tastes) as well as one-loop matching factors. These results are provided in Refs. [29, 30]. Finally, we need to evolve matrix elements using the continuum renormalization group for $\Delta S = 2$ operators. The required two-loop anomalous dimensions were calculated in Ref. [31], and some additional technical details are worked out in Ref. [30].

This paper is organized as follows. In Sec. II, we describe the basis of $\Delta S = 2$ four-quark operators that we use, and the corresponding B-parameters and gold-plated combinations. In Sec. III, we describe the details of the lattice calculation. We next turn to the analysis. Sec. IV explains how we extrapolate valence quark masses to their physical values, while Sec. V describes the combined extrapolation to the continuum limit and to physical sea-quark masses. We present our final results and error budget in Sec. VI, and compare these to the above-mentioned results that use other fermion discretizations in Sec. VII.

II. $\Delta S = 2$ FOUR-QUARK OPERATORS AND BAG PARAMETERS

We use the operator basis (Buras's basis) of Ref. [31], in which the $\Delta S = 2$ four-quark operators are

$$Q_1 = [\bar{s}^a \gamma_\mu (1 - \gamma_5) d^a][\bar{s}^b \gamma_\mu (1 - \gamma_5) d^b] ,$$
$$Q_2 = [\bar{s}^a (1 - \gamma_5) d^a][\bar{s}^b (1 - \gamma_5) d^b] ,$$
$$Q_3 = [\bar{s}^a \sigma_{\mu\nu} (1 - \gamma_5) d^a][\bar{s}^b \sigma_{\mu\nu} (1 - \gamma_5) d^b] , \quad (1)$$
$$Q_4 = [\bar{s}^a (1 - \gamma_5) d^a][\bar{s}^b (1 + \gamma_5) d^b] ,$$
$$Q_5 = [\bar{s}^a \gamma_\mu (1 - \gamma_5) d^a][\bar{s}^b \gamma_\mu (1 + \gamma_5) d^b] .$$

Here the operators have been written in Euclidean space, with a and b being color indices. Q_1 is the operator corresponding to B_K, while $Q_{2,3,4,5}$ are the BSM operators.[2]

The hadronic matrix elements of the $\Delta S = 2$ four-quark operators can be parametrized by so-called kaon bag parameters (or B-parameters). These are conventionally defined by

$$B_K = \frac{\langle \overline{K}_0 | Q_1 | K_0 \rangle}{\frac{8}{3} \langle \overline{K}_0 | \bar{s} \gamma_\mu \gamma_5 d | 0 \rangle \langle 0 | \bar{s} \gamma_\mu \gamma_5 d | K_0 \rangle} \quad (2)$$

$$B_j = \frac{\langle \overline{K}_0 | Q_j | K_0 \rangle}{N_j \langle \overline{K}_0 | \bar{s} \gamma_5 d | 0 \rangle \langle 0 | \bar{s} \gamma_5 d | K_0 \rangle} , \quad (3)$$

where $j = 2 - 5$, and

$$(N_2, \ N_3, \ N_4, \ N_5) = (5/3, \ 4, \ -2, \ 4/3) \quad (4)$$

---

[2] This basis is complete in four dimensions aside from the need to add the parity conjugates of $Q_1 - Q_3$. We do not consider these additional operators, however, since they have the same positive parity parts as $Q_1 - Q_3$, and the matrix element we consider picks out the positive parity parts.

are factors arising in the vacuum saturation approxima-
tion. In the following, we will often refer collectively
to "the B_i", and this will indicate all five of the B-
parameters, i.e. the index i runs over $i = K, 2, 3, 4, 5$.

In our lattice calculation, we find it more convenient
to evaluate the B-parameters rather than the correspond-
ing matrix elements, $\langle \overline{K}_0 | Q_i | K_0 \rangle$. This avoids the need
to determine the overlap of our sources with the $\overline{K}_0$ and
K_0 states, reduces the dependence on the scale, a, since
the B-parameters are dimensionless, cancels some of sta-
tistical and systematic errors, and simplifies chiral ex-
pansions, since the staggered chiral perturbation theory
(SChPT) expressions are simpler [28].

We also make extensive use of "gold-plated" combi-
nations of the B-parameters. These are combinations
chosen to be free of chiral logarithms at next-to-leading
order (NLO) in SU(2) chiral perturbation theory [28]:

$$G_{21} \equiv \frac{B_2}{B_K}, \quad G_{23} \equiv \frac{B_2}{B_3},$$
$$G_{24} \equiv B_2 \cdot B_4, \quad G_{45} \equiv \frac{B_4}{B_5}. \tag{5}$$

In this paper, the subindex i of the G_i runs over $i = 21, 23, 24, 45$.

As described below, it turns out that the combined ex-
trapolation in a^2 and sea-quark masses is much better
controlled for the G_i and B_K than for B_{2-5}. Thus our fi-
nal results for the BSM B-parameters are obtained using
B_K and the G_i in the following way:

$$B_2^G = B_K \cdot G_{21},$$
$$B_3^G = B_K \cdot \frac{G_{21}}{G_{23}},$$
$$B_4^G = \frac{G_{24}}{B_K \cdot G_{21}}, \tag{6}$$
$$B_5^G = \frac{G_{24}}{B_K \cdot G_{21} \cdot G_{45}}.$$

The superscript G indicates that we use gold-plated com-
binations to reconstruct the B-parameters.

III. LATTICES AND MEASUREMENTS

We use the MILC ensembles listed in Table I. These are
generated with $N_f = 2 + 1$ flavors of staggered fermions
using the "asqtad" fermion action. Details of the con-
figuration generation are given in Ref. [32]. To convert
our data to physical units, we use the values of r_1/a
obtained by the MILC collaboration. [32, 33], and set
$r_1 = 0.3117(22)$ fm, following Refs. [33, 34].[3] We stress

---

[3] Some values of r_1/a are updated compared to Ref. [32]; these are
F2: 3.6987, F3: 3.7036, F4: 3.7086, F5:3.6993, F7: 3.7000, F9:
3.6984, S4: 5.2825, S5: 5.2836 [33].

TABLE I. MILC ensembles used in our numerical study. Here
"ens" represents the number of gauge configurations, "meas"
is the number of measurements per configuration, and ID is
a label. am_ℓ and am_s are, respectively, the light and strange
sea quark masses in lattice units. The values of a are nominal.

a (fm)	am_l/am_s	size	ens $\times$ meas	ID
0.12	0.03/0.05	$20^3 \times 64$	564×9	C1
0.12	0.02/0.05	$20^3 \times 64$	486×9	C2
0.12	0.01/0.05	$20^3 \times 64$	671×9	C3
0.12	0.01/0.05	$28^3 \times 64$	274×8	C3-2
0.12	0.007/0.05	$20^3 \times 64$	651×10	C4
0.12	0.005/0.05	$24^3 \times 64$	509×9	C5
0.09	0.0062/0.031	$28^3 \times 96$	995×9	F1
0.09	0.0031/0.031	$40^3 \times 96$	959×9	F2
0.09	0.0093/0.031	$28^3 \times 96$	949×9	F3
0.09	0.0124/0.031	$28^3 \times 96$	1995×9	F4
0.09	0.00465/0.031	$32^3 \times 96$	651×9	F5
0.09	0.0062/0.0186	$28^3 \times 96$	950×9	F6
0.09	0.0031/0.0186	$40^3 \times 96$	701×9	F7
0.09	0.00155/0.031	$64^3 \times 96$	790×9	F9
0.06	0.0036/0.018	$48^3 \times 144$	749×9	S1
0.06	0.0025/0.018	$56^3 \times 144$	799×9	S2
0.06	0.0072/0.018	$48^3 \times 144$	593×9	S3
0.06	0.0054/0.018	$48^3 \times 144$	582×9	S4
0.06	0.0018/0.018	$64^3 \times 144$	572×9	S5
0.045	0.0028/0.014	$64^3 \times 192$	747×1	U1

that the values of a listed in the table are nominal. The
actual values (determined from r_1/a) differ slightly from
the nominal values, and it is the former that we use in
our analysis. In the following, we sometimes use MILC
terminology and refer to the sets of ensembles with nom-
inal lattice spacings of $a = 0.12$ fm, 0.09 fm, 0.06 fm and
0.045 fm as coarse, fine, superfine and ultrafine lattices,
respectively.

Compared to the results presented in Ref. [23], the
additional ensembles are F6, F7, F9 and S5. These ad-
ditions significantly improve the reliability of the chiral
extrapolations, as we now explain. On all ensembles ex-
cept F6 and F7, the strange sea quark masses lie close
to, but not exactly at, the physical value. Adding in F6
and F7, which have lighter strange sea quarks, allows us
to correct for the offset. Adding S5 ensures that on both
fine and superfine lattices the average up/down sea quark
mass, m_ℓ, ranges down to $\approx m_s^{\text{phys}}/10$, so that the chiral
extrapolation is relatively short. Finally, adding in F9
provides us with a light sea quark mass, $m_\ell \approx m_s^{\text{phys}}/20$,
that lies much closer to the physical value.

We use HYP-smeared staggered fermions [35] as va-
lence quarks. Parameters for the HYP smearing are cho-
sen to remove $\mathcal{O}(a^2)$ taste-symmetry breaking at tree
level [36]. We use 10 different valence quark masses on
each lattice:

$$m_x, \ m_y = m_s^{\text{nom}} \times \frac{n}{10} \qquad \text{with } n = 1, 2, 3, \ldots, 10, \tag{7}$$

where $m_s^{\rm nom}$ is the nominal strange quark mass given in Table II. We have labeled the valence masses m_x and m_y, the former corresponding to the valence d quark and the latter to the valence s quark.

As explained in the next section, m_x and m_y will be extrapolated to their physical values, $m_d^{\rm phys}$ and $m_s^{\rm phys}$, respectively. To determine these physical values on each ensemble use the same method as in Ref. [7]. First, the flavor non-singlet $y\bar{y}$ "pion" mass is extrapolated until is equals $M_{ss,\rm phys} = 0.6858(40)$ GeV, which is the "physical" value determined in Ref. [37]. This determines $m_s^{\rm phys}$. Second, m_x is extrapolated (with m_y at its now-determined physical value) such that the $x\bar{y}$ "kaon" has a mass equal to that of the physical K_0. These extrapolations are done separately on each ensemble. For illustration, we show in Table II the resulting physical values (as well as the valence masses we use in the simulations) for the ensembles having $m_\ell/m_s = 1/5$. We see that our lightest valence quark masses are roughly twice $m_d^{\rm phys}$, while our heaviest lie somewhat below $m_s^{\rm phys}$.

TABLE II. Physical values of valence quark masses on representative ensembles, in lattice units. For comparison, we also show the range of valence masses used in simulations.

Ensemble	$am_d^{\rm phys}$	$am_s^{\rm phys}$	am_x and am_y
C3	0.00213(2)	0.05204(5)	0.005–0.05
F1	0.00146(2)	0.03542(5)	0.003–0.03
S1	0.00104(1)	0.02372(3)	0.0018–0.018
U1	0.00076(1)	0.01693(3)	0.0014–0.014

We calculate the valence $x\bar{x}$ "pion" and $x\bar{y}$ "kaon" masses in standard fashion using the same wall sources as described below. The statistical errors on these results are very small. In Table III we quote some representative values to indicate the range of pion masses in physical units. Note that $m_\pi(\rm val, max)$ is the mass of the heaviest pion that we use in our chiral extrapolation to the physical valence d quark. This extrapolation is discussed in the following section. We also include values for the lightest sea-quark pion for the fine, superfine and ultrafine lattices, as well as for the coarse ensemble that we use to study finite-volume effects.

We use essentially the same methodology for calculating the BSM B-parameters as we employed in the calculation of B_K in Ref. [7]. Thus we give only a brief discussion here, while for B_K we refer to Ref. [7]. In terms of lattice operators, the BSM B-parameters are

$$B_j(t) = \frac{2\langle \overline{K}_{P1}^0 | z_{jk} Q_k^{\rm Lat}(t) | K_{P2}^0 \rangle}{N_j \langle \overline{K}_{P1}^0 | z_P \mathcal{O}_P^{\rm Lat}(t) | 0 \rangle \langle 0 | z_P \mathcal{O}_P^{\rm Lat}(t) | K_{P2}^0 \rangle}, \quad (8)$$

where $Q_k^{\rm Lat}$ are lattice four-fermion operators and $\mathcal{O}_P^{\rm Lat}$ is the taste ξ_5 pseudoscalar bilinear. z_{jk} and z_P are one-loop matching factors that convert lattice operators to their continuum counterparts, the latter defined in the $\overline{\rm MS}$ scheme using naive dimensional regularization

(NDR). We use the mean-field improved lattice operators defined in Refs. [29, 30]. The one-loop matching is quite involved as one must ensure that the continuum basis is extended to $d = 4 - 2\epsilon$ dimensions using the same definition of evanescent operators as in Ref. [31]. The matching factors have been worked out and described in detail in Ref. [30], building on the earlier work of Ref. [29], and we do not repeat them here. They depend on the renormalization scale μ of the continuum operator and on α_s. The latter is chosen to be in the $\overline{\rm MS}$ scheme and is evaluated at the same scale μ. In our initial matching we take $\mu = 1/a$ and then evolve the results in the continuum to a common renormalization scale. In the numerical evaluation of the matching coefficients we use four loop running to determine $\alpha_s(\mu)$, using as input $\alpha_s(M_Z) = 0.118$.

To produce the kaons and antikaons, we place U(1)-noise wall sources on time slices t_1 and t_2, with $t_2 > t_1$. These produce taste ξ_5 kaons and anti-kaons having zero spatial momenta. The four-quark operators are placed between the sources at time t (i.e. $t_1 < t < t_2$). When t is far enough from the sources, so that excited state contamination is small, the three-point correlators should be independent of t, and can be fit to a constant. To determine the fit range, we use the two-point correlator from the wall-source to the taste ξ_5 axial current. From the effective mass plot for this correlator, we find the distance from the source, t_L, for which the contamination from excited states becomes negligibly small. Then we fit from $t = t_1 + t_L$ to $t = t_1 + t_R = t_2 - t_L - 1$ (which is a symmetrical range since our operators extend over the two time slices t and $t + 1$). Our choices of t_L and t_R are given in Table IV. Note that we choose $\Delta t = t_2 - t_1$ to be less than half of the time extent of the lattice to avoid "around the world" contributions. Further details concerning sources and time ranges is given in Ref. [7].

The plateaus resulting from the above-described procedure are reasonable. Examples are shown for the gold-plated combinations G_{23} and G_{45} in Figs. 1 and 2. Here we show cases with light valence quark masses ($m_x/m_y = 1/10$ with $m_l/m_s = 1/5$) for which the statistical errors are larger. The fits to a constant are per-

TABLE III. Valence and sea pion masses (in GeV) on representative ensembles. $m_\pi(\rm val, min)$ and $m_\pi(\rm val, max)$ are the minimum and maximum valence pion masses used in our valence chiral extrapolation. The values for these quantities on other coarse, fine and superfine ensembles are very similar to those on ensembles C3, F9 and S5, respectively. For the fine, superfine and ultrafine lattices, we show the sea quark pion mass on the ensemble with the smallest value of this quantity. For the coarse lattices, we pick the ensemble used to estimate finite-volume effects.

Ensemble	$m_\pi(\rm val, min)$	$m_\pi(\rm val, max)$	$m_\pi(\rm sea)$
C3	0.222	0.430	0.372
F9	0.206	0.401	0.174
S5	0.195	0.379	0.222
U1	0.206	0.397	0.316

TABLE IV. Choices for the wall source separation, $\Delta t = t_2 - t_1$, and its ratio to the temporal length of the lattices, T, as well as the parameters determining the fitting range.

lattice spacing	Δt	$\Delta t/T$	t_L	t_R	t_L (fm)
0.12 fm	26	0.41	10	15	1.19
0.09 fm	40	0.42	14	25	1.18
0.06 fm	60	0.42	22	37	1.29
0.045 fm	80	0.42	26	53	1.14

formed ignoring correlations between time slices (diagonal approximation for the covariance matrix) in order to avoid instabilities due to the small eigenvalues of the covariance matrix [38]. Fitting errors are estimated using the jackknife method.

To increase statistics, we do multiple measurements on each configuration. For each measurement, the source position t_1 is chosen randomly, with t_2 determined by $t_2 = t_1 + \Delta t$, where Δt is the wall-source separation listed in Table IV. In addition, we use different random numbers for the wall sources for each measurement. The number of measurements for each gauge configuration is listed in Table I.

To study auto-correlations we bin adjacent lattices in the Markov chain and study the dependence of the nominal statistical error on bin size. Examples of the results are shown in Fig. 3. The notation for the operators used in this figure is explained in Refs. [29, 30]. We find that the auto-correlations increase as the lattice spacing decreases. As one can see from Fig. 3, the auto-correlation effect is about 100% for the MILC superfine lattice S1, while it is about 25% for the MILC fine lattice F1. In order to greatly reduce the effects of auto-correlations, we use bins of size 5 throughout our analysis.

IV. CHIRAL EXTRAPOLATION

Our analysis follows the same steps as in Refs. [9, 23]. The first step is the chiral extrapolation of the valence quark masses to their physical values. We extrapolate m_x to the m_d^{phys} for fixed m_y using a fitting form based on SU(2) SChPT, and then extrapolate m_y to m_s^{phys}. For SU(2) ChPT to be valid, we require that $m_x \ll m_y$. Hence, from the 10 valence quark masses listed in Eq. (7), we take the lightest four for m_x (e.g. $m_x = \{0.003,\ 0.006,\ 0.009,\ 0.012\}$ on the fine ensemble) and heaviest three for m_y (e.g. $m_y = \{0.024,\ 0.027,\ 0.03\}$ on the fine ensemble). In this way we satisfy $m_x \leq m_y/2$.

We begin by considering the extrapolation in m_x, which we call the "X fit". The actual extrapolation is done in $X_P = m_{xx,P}^2$, which is the squared mass of the $x\bar{x}$ valence pion with taste ξ_5 (i.e. the Goldstone pion). For the physical value of this quantity we take $X_P = 2M_{K_0,\text{phys}}^2 - M_{ss,\text{phys}}^2 = (0.158\ \text{GeV})^2$. At next-to-leading order (NLO) in SU(2) SChPT, the light valence quark mass dependence of the B-parameters has been worked out in Ref. [28], and is

$$B_i(\text{NLO}) = c_1 F_0(i) + c_2 X, \qquad (9)$$

where $X \equiv \dfrac{X_P}{\Lambda_\chi^2}$ with $\Lambda_\chi = 1\ \text{GeV}$, the c_j are coefficients to be determined, and

$$F_0(i) = 1 \pm \frac{1}{32\pi^2 f^2}\left\{ \ell(X_I) + (L_I - X_I)\tilde{\ell}(X_I) \right.$$
$$\left. - \frac{1}{16}\sum_B \ell(X_B)\right\}, \quad (10)$$

is the chiral logarithm. Here X_B (L_B) is the squared mass of the taste B, flavor non-singlet, pion composed of two light valence (sea) quarks: $X_B = m_{xx,B}^2$ ($L_B = m_{ll,B}^2$). The functions $\ell(X)$ and $\tilde{\ell}(X)$ are chiral logarithms defined, for example, in Ref. [28]. In Eq. (10), the plus sign applies for $i = K, 2, 3$, and the minus sign for $i = 4, 5$.

The NLO fitting function is not accurate enough to describe the precise and highly correlated data. Hence, as in all our recent analyses [8, 9, 23], we add higher order terms to the fitting function:

$$B_j(\text{NNNLO}) = c_1 F_0(j) + c_2 X + c_3 X^2 + c_4 X^2 \ln^2(X)$$
$$+ c_5 X^2 \ln(X) + c_6 X^3. \qquad (11)$$

The three terms $X^2, X^2\ln^2(X)$ and $X^2\ln(X)$ are the generic NNLO terms in continuum chiral perturbation theory. We also add a single analytic NNNLO term proportional to X^3. We use a similar fitting function for the X fits of gold-plated combinations, except that, by construction, there are no NLO chiral logarithms:

$$G_i(\text{NNNLO}) = c_1 + c_2 X + c_3 X^2 + c_4 X^2 \ln^2(X)$$
$$+ c_5 X^2 \ln(X) + c_6 X^3. \qquad (12)$$

We have found that adding yet higher order terms in the chiral expansion does not improve the fits to either the B_i or G_i.

Since we have only four data points for the X fit, we use the Bayesian method [39], and place constraints on the three higher-order fitting parameters c_{4-6}. Our prior information is that these coefficients are of $\mathcal{O}(1)$. We thus first impose the constraints $c_{4-6} = 0 \pm 1$. If the resulting fits have $\chi^2/\text{d.o.f.} \lesssim 1$, then we accept them. If not, we try the less restrictive constraints $c_{4-6} = 0 \pm 2$. Again, we accept fits with $\chi^2/\text{d.o.f.} \lesssim 1$, but otherwise fit again using $c_{4-6} = 0 \pm 4$. In all cases this leads to fits having $\chi^2/\text{d.o.f.} \lesssim 1$. In this discussion, the χ^2 that is minimized is the augmented version:

$$\chi_{\text{aug}}^2 = \chi^2 + \chi_{\text{prior}}^2, \qquad (13)$$

$$\chi_{\text{prior}}^2 = \sum_{i=4}^{6} \frac{(c_i - a_i)^2}{\sigma_i^2}, \qquad (14)$$
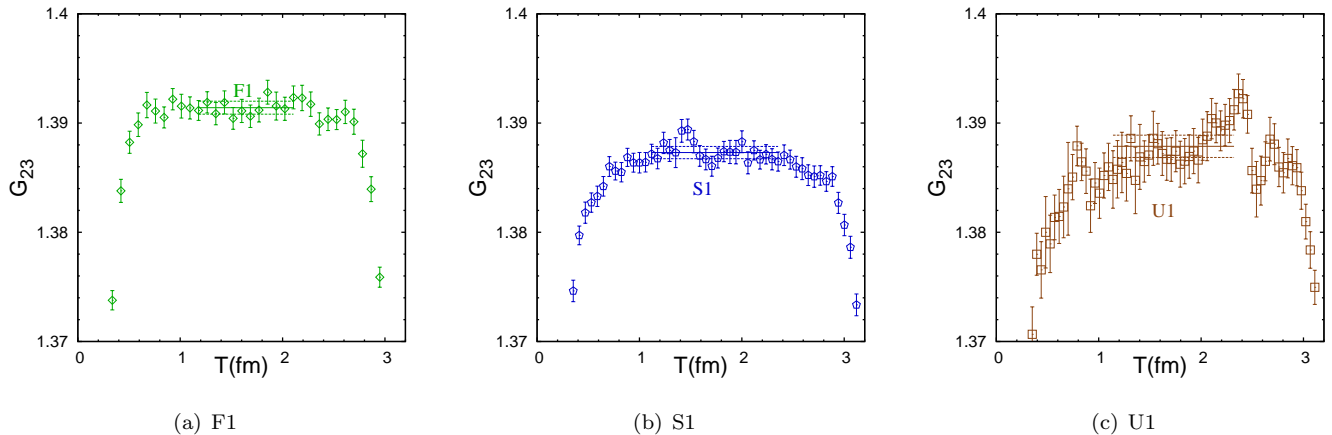
(a) F1

(b) S1

(c) U1

FIG. 1. G_{23} (evaluated at renormalization scale $\mu = 1/a$ as a function of $T = t - t_1$. Green diamonds show on the F1 ensemble with $(am_x, am_y) = (0.003, 0.03)$. Blue pentagons are results from the S1 ensemble with $(am_x, am_y) = (0.0018, 0.018)$. Brown squares are results on the U1 ensemble with $(am_x, am_y) = (0.0014, 0.014)$. The fit ranges (and resulting central values and error bands) are shown by the horizontal lines.
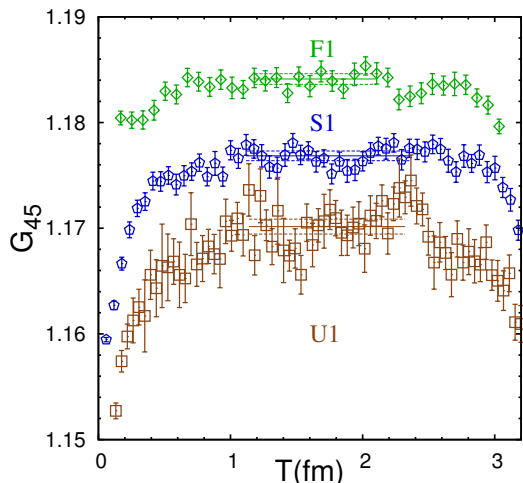

FIG. 2. G_{45} as a function of $T = t - t_1$ at $\mu = 1/a$. The convention for symbols is as in Fig. 1.

where we set $a_i = 0$ and $\sigma_i = 1, 2, 4$. These fits are done using the full correlation matrix, and have acceptable values of χ^2.

Having determined the parameters c_{1-6}, we extrapolate the results to the physical point $m_x = m_d^{\mathrm{phys}}$, and simultaneously remove (by hand) the lattice artifacts that lead to taste symmetry breaking in pion masses. Specifically, within the chiral logarithm $F_0(i)$ we set X_B and L_I to their physical values, as explained in Ref. [7]. In this way we are using knowledge from SChPT to remove a significant source of discretization errors. Note that this correction applies to the B_i but not to the G_j, since the gold-plated combinations have no chiral logarithms

at NLO.

Examples of the X fits are shown in Figs. 4(a), 5(a), and 6(a), for B_K, G_{23} and G_{45}, respectively. In all these fits it was sufficient to use the narrowest range of the Bayesian priors ($\sigma_i = 1$) in order to obtain good fits. We note that the statistical errors appear larger in the results for G_{23} because of the finer vertical scale. The figures emphasize the fact that the extrapolation in X_P is relatively short. Thus the dependence on SChPT is relatively mild, except for the taste-breaking correction that we make to B_K.

In order to estimate the systematic uncertainty in the X fits we consider two variations in the fitting scheme. The first error is obtained from the changes in the B_i and G_j when the prior widths σ_a are doubled. The second is obtained by repeating the fits keeping only one NNLO term,

$$B_K(\mathrm{NNLO}) = c_1 F_0(K) + c_2 X + c_3 X^2, \qquad (15)$$
$$G_i(\mathrm{NNLO}) = c_1 + c_2 X + c_3 X^2, \qquad (16)$$

and using the eigenmode shift (ES) method introduced in Ref. [38]. The ES method tunes the fitting function in the direction of the eigenvectors of the covariance matrix corresponding to the small eigenvalues, with small shifting parameters η that are constrained by the Bayesian prior condition: $\eta = 0 \pm \sigma_\eta$. We set σ_η from the size of the neglected highest order term in the fitting function,

$$\sigma_\eta = 0.006 \approx X^2 (\ln(X))^2, \qquad (17)$$

where $X \approx 0.02$.

The total systematic error from the X fits is then obtained by adding these two error estimates in quadrature. The resulting errors are discussed in Sec. VI.

We next extrapolate m_y to m_s^{phys}, using the three heaviest values of the valence quark masses. This we denote

(a) $[P \times P][P \times P]_I$
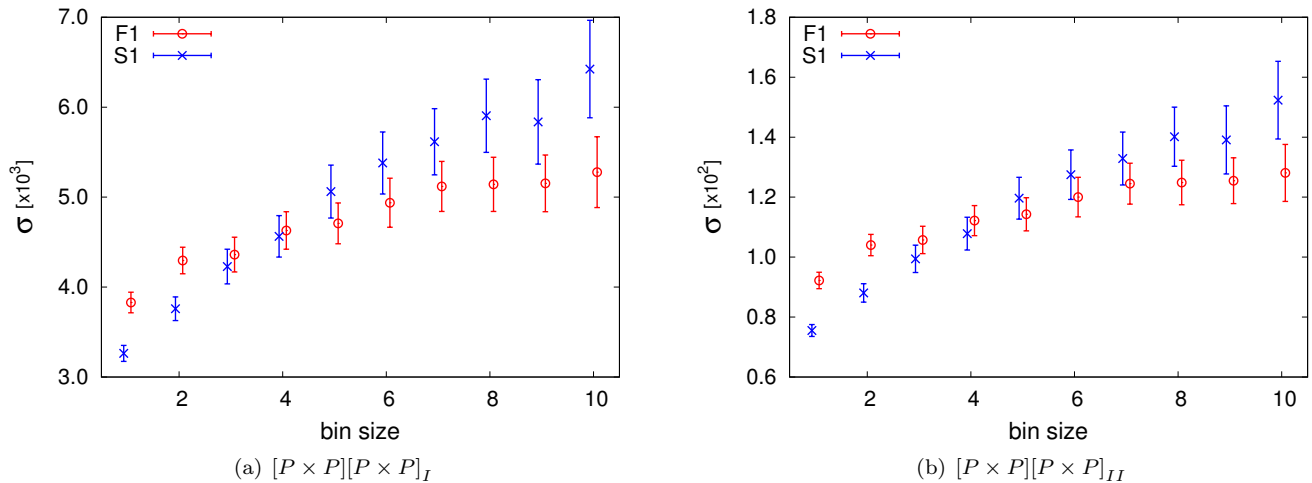

(b) $[P \times P][P \times P]_{II}$

FIG. 3. Statistical errors for bare three-point functions as a function of bin size. The operators are (a) $\mathcal{O}_{P1}^{\text{Lat}}$, and (b) $\mathcal{O}_{P2}^{\text{Lat}}$, respectively, at $T = 20$ (F1) and $T = 30$ (S1). (Red) circles are the results on F1 ensemble, with $(am_x, am_y) = (0.003, 0.03)$; and (blue) crosses are the results on S1 ensemble, with $(am_x, am_y) = (0.0018, 0.018)$.
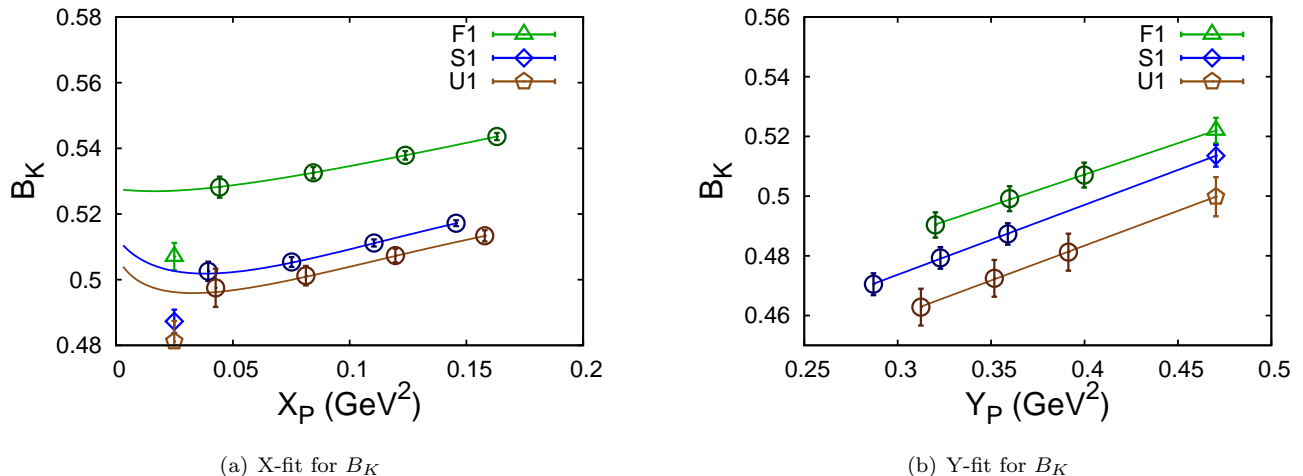

(a) X-fit for B_K

(b) Y-fit for B_K

FIG. 4. (a) X fits and (b) Y fits for B_K evaluated at $\mu = 1/a$ on the F1, S1 and U1 ensembles. The valence strange-quark masses are $am_y = 0.03$, 0.018 and 0.014, respectively. Lattice results are shown with circles (green, blue and brown for F1, S1, and U1, respectively) and are ordered vertically as shown in the legend. Extrapolated results are shown with [green] triangles (F1), [blue] diamonds (S1) and [brown] pentagons (U1). For the X fit, the extrapolated results lie below the curves because of the removal of taste-breaking effects, as described in the text.

the "Y fit". We expect the B_i and G_j to be smooth, analytic functions of Y_P, since the strange quark is far from the chiral limit. Empirically, linear fitting works very well, as illustrated in Figs. 4(b), 5(b) and 6(b). To avoid the problem of small eigenvalues, we use uncorrelated fitting for the Y fits. In all cases, fits are stable and the fit parameters are consistent across all lattices with a given nominal lattice spacing (within the statistical uncertainties). To estimate the systematic error in the results of the Y fits, we repeat the fits using a quadratic function of Y_P. The changes in the final results for B_i and G_j are then taken as the systematic error.

V. CONTINUUM-CHIRAL EXTRAPOLATION

The outputs of the extrapolations in valence masses are values for the B-parameters and gold-plated combinations on each ensemble, for continuum operators evaluated at the renormalization scale $\mu = 1/a$. In order to compare these results and extrapolate them to the continuum limit, and to physical sea-quark masses, we must use renormalization group (RG) evolution to evolve to a common scale. The standard choices for this scale in the literature are $\mu = 2$ GeV and $\mu = 3$ GeV, and we present results for both. Since we use one-loop matching, to do
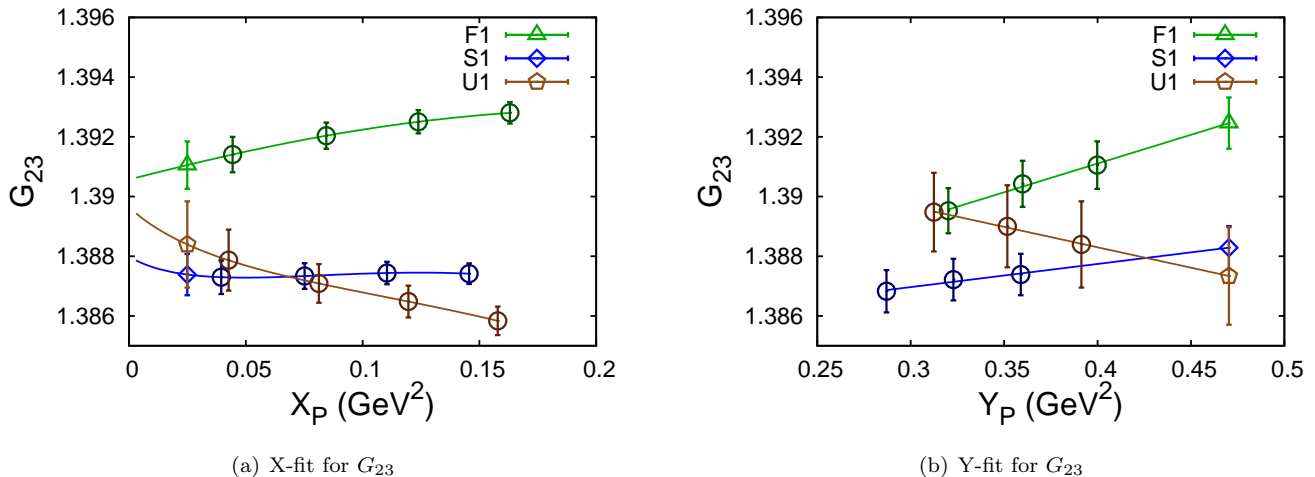
(a) X-fit for G_{23}

(b) Y-fit for G_{23}

FIG. 5. (a) X fits and (b) Y fits for G_{23}. Notation as in Fig. 4, except that for the gold-plated combinations there is no taste-breaking correction.
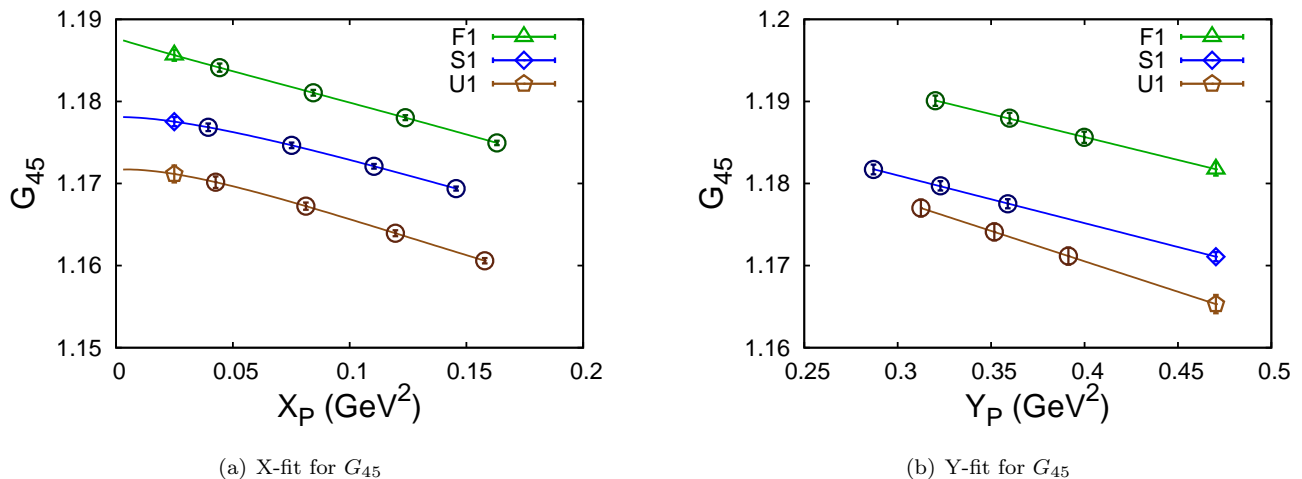

(a) X-fit for G_{45}

(b) Y-fit for G_{45}

FIG. 6. (a) X fits and (b) Y fits for G_{45}. Notation as in Fig. 4.

the running consistently we need the continuum two-loop anomalous dimension matrix. This has been calculated in Ref. [31] for a particular choice of evanescent operators. Because of this, it is essential that our lattice-continuum matching uses the same set of evanescent operators, as is indeed the case in Ref. [30]. Some technical issues arise in the RG running; these are described in Ref. [30] along with our resolutions.

We present our results for B_K and the gold-plated combinations G_i at the two renormalization scales in Tables V and VI. Statistical errors range from the percent level to an order of magnitude smaller. We have also obtained results for the B_j ($j = 2 - 5$) but do not show these as they are not used in our final analysis.

The final step of our analysis is to do a simultaneous extrapolation to the physical values of the sea-quark masses and to the continuum limit. We call this proce-

dure "the continuum-chiral extrapolation", although this name is slightly misleading as the valence chiral extrapolation has already been done. As substitutes for sea quark masses, we use L_P and S_P, which are, respectively, the squared masses of taste-ξ_5 (Goldstone) pions composed of two light sea quarks ($l\bar{l}$) and two strange sea quarks ($s\bar{s}$). They are extrapolated to their physical values, which we take to be $m_{\pi_0}^2 = (0.1349766\,\text{GeV})^2$ for L_P and $M_{ss,\text{phys}}^2 = (0.6858\,\text{GeV})^2$ for S_P [37].

We expect the dependence of the B_i and G_j on L_P, S_P and a^2 to be analytic, with terms organized according to standard SChPT power counting. At NLO, the only term in SChPT that could violate this expectation is the chiral logarithm. This is absent for the G_j. For the B_i, as shown by Eq. (10), the only logarithms that appear have the schematic dependence $(L_P + a^2) \log X_B$ and $X_B \log X_B$. Since X_B is set by hand to its physical

TABLE V. B_K and gold-plated combinations for $\mu = 2\,\text{GeV}$ on each lattice listed in Table I. The superscripts indicate whether broadened Bayesian priors have been used in the X-fits: † implying $c_{4-6} = 0 \pm 2$, while ‡ implying $c_{4-6} = 0 \pm 4$. Results without superscripts are obtained with $c_{4-6} = 0 \pm 1$.

ID	B_K	G_{21}	G_{23}	G_{24}	G_{45}
C1	0.5484(55)	0.995(11)†	1.4140(10)	0.6205(19)	1.1836(7)
C2	0.5528(56)	0.993(11)†	1.4119(11)	0.6232(22)	1.1824(8)
C3	0.5673(52)	0.975(10)‡	1.4098(9)	0.6256(20)	1.1819(7)
C3-2	0.5715(51)	0.974(9)†	1.4105(9)	0.6229(16)	1.1823(6)
C4	0.5641(54)	0.987(11)‡	1.4113(9)	0.6291(19)	1.1822(6)
C5	0.5677(46)	0.976(8)†	1.4082(8)	0.6264(15)	1.1834(5)
F1	0.5294(43)	1.0451(69)	1.4000(10)	0.6092(19)	1.2003(9)
F2	0.5451(35)	1.0281(59)	1.3985(6)	0.6088(11)	1.1993(5)
F3	0.5226(49)	1.053(10)†	1.4015(11)	0.6119(21)	1.1991(10)
F4	0.5255(30)	1.0366(64)‡	1.4033(7)	0.6050(12)	1.2008(6)
F5	0.5388(43)	1.0322(84)†	1.3995(9)	0.6101(17)	1.1997(8)
F6	0.5472(59)†	1.014(11)‡	1.3991(13)	0.6123(23)	1.2018(9)
F7	0.5392(35)	1.0394(59)	1.3953(7)	0.6130(12)	1.1992(6)
F9	0.5501(16)	1.0258(30)	1.3976(3)	0.6093(6)	1.1991(3)
S1	0.5359(38)	1.0531(55)	1.4140(10)	0.5858(17)	1.2288(8)
S2	0.5361(36)	1.0423(57)	1.4116(9)	0.5833(13)	1.2278(8)
S3	0.5261(41)†	1.0625(79)‡	1.4184(13)	0.5842(20)	1.2278(10)
S4	0.5204(33)	1.0621(60)	1.4124(10)	0.5820(18)	1.2277(8)
S5	0.5384(36)	1.0446(55)	1.4110(8)	0.5835(12)	1.2287(8)
U1	0.5325(70)	1.056(11)	1.4302(28)	0.5718(39)	1.2539(19)

TABLE VI. B_K and gold-plated combinations for $\mu = 3\,\text{GeV}$ on each lattice listed in Table I. The convention for † and ‡ is the same as Table V.

ID	B_K	G_{21}	G_{23}	G_{24}	G_{45}
C1	0.5298(53)	0.951(10)†	1.3942(8)	0.5713(18)	1.1468(6)
C2	0.5341(54)	0.950(10)†	1.3926(8)	0.5738(20)	1.1459(6)
C3	0.5481(50)	0.9323(97)‡	1.3911(7)	0.5760(19)	1.1455(5)
C3-2	0.5521(49)	0.9308(89)†	1.3915(7)	0.5735(14)	1.1458(5)
C4	0.5449(52)	0.944(10)‡	1.3921(7)	0.5792(18)	1.1457(5)
C5	0.5484(45)	0.9327(80)†	1.3898(6)	0.5767(14)	1.1467(4)
F1	0.5115(42)	0.9991(66)	1.3829(7)	0.5610(18)	1.1594(7)
F2	0.5266(34)	0.9828(56)	1.3817(5)	0.5606(10)	1.1586(4)
F3	0.5049(47)	1.0069(96)†	1.3840(9)	0.5634(19)	1.1584(8)
F4	0.5077(29)	0.9909(61)‡	1.3853(5)	0.5571(11)	1.1597(4)
F5	0.5205(42)	0.9867(80)†	1.3825(6)	0.5618(16)	1.1589(6)
F6	0.5287(57)†	0.969(10)‡	1.3821(10)	0.5639(21)	1.1604(7)
F7	0.5210(34)	0.9935(56)	1.3793(5)	0.5645(11)	1.1585(5)
F9	0.5314(16)	0.9806(29)	1.3811(3)	0.5611(5)	1.1585(2)
S1	0.5178(37)	1.0068(53)	1.3927(8)	0.5394(16)	1.1806(6)
S2	0.5179(34)	0.9965(55)	1.3909(7)	0.5372(12)	1.1798(6)
S3	0.5083(39)†	1.0158(76)‡	1.3960(10)	0.5380(19)	1.1798(8)
S4	0.5028(31)	1.0153(58)	1.3916(8)	0.5359(16)	1.1797(6)
S5	0.5202(34)	0.9986(53)	1.3905(6)	0.5373(12)	1.1805(6)
U1	0.5145(67)	1.009(10)	1.4044(21)	0.5266(36)	1.1991(14)

value, the a^2 dependence it contains is removed. The remaining dependence on L_P and a^2 is analytic, and in fact also is removed by hand when we set L_P to its physical value and a^2 to zero. Chiral logarithms of higher order can lead to non-analyticities, or large derivatives, but these are numerically suppressed. Thus, to good approximation, we expect all the quantities we calculate to be described by

$$\tilde{F}_1 = d_1 + d_2 \frac{L_P}{\Lambda_\chi^2} + d_3 \frac{S_P - M_{ss,\text{phys}}^2}{\Lambda_\chi^2} + d_4 (a\Lambda_Q)^2 . \quad (18)$$

Here $\Lambda_Q = 0.3$ GeV and $\Lambda_\chi = 1$ GeV, and we have chosen to expand the d_3 term about the physical $s\bar{s}$ mass. When we fit our results to this form, we impose

Bayesian constraints on the linear terms to enforce the expected power counting: $d_{2-4} = 0 \pm 2$. We have also tried fits with broader contraints, $d_{2-4} = 0 \pm 4$, but find that these do not significantly change the χ^2 or the resulting fit parameters. We find, as was the case in our earlier work [8, 9, 23] that we cannot obtain a good description if we include the coarse lattices. Thus we fit all the fine, superfine and ultrafine lattice data to Eq. (18). We call this the $\tilde{F}_1$ fit, since it is a small variation from the fitting function F_B^1 in our previous work [9] (differing only in the offset in the d_3 term). Since the number of configurations differ on each ensemble, errors on the fit parameters are obtained using a variant of the bootstrap method. Note that for this fit there are no correlations between the different ensembles.

In Table VII, we show the results of the $\tilde{F}_1$ fits to B_K and the G_i (renormalized at $\mu = 2\,\text{GeV}$). Plots of the fits are shown in Figs. 7(a), 8(a), 9(a), 10(a), and 11(a). The fits are qualitatively similar and of comparable quality if the operators are renormalized at $\mu = 3\,\text{GeV}$. To interpret these plots the following must be kept in mind. For each nominal value of a (e.g. for the fine lattices) there is a variation in the actual values of a and in the values of S_P. This is most significant for the ensembles F6 and F7, which have a substantially lower strange quark mass than the other fine ensembles. These variations are accounted for in the fit (with F6 and F7 providing a significant lever arm to determine d_3), but *do not show up in these two-dimensional plots.* Indeed, the points from F6 and F7 are not included in the plots, while the fit lines for the fine and superfine ensembles are shown with a and S_P set to their average values (excluding ensembles F6 and F7 for the fine lattices). Thus, even if the fit were perfect, the fit lines would not pass through any of the points, except for the ultrafine case. Because of this, the fits appear slightly worse than they actually are; the real indicator of goodness of each fit is the quoted value of χ^2/d.o.f..

The fits indicate that the dependence on the strange sea-quark mass is very weak for all five quantities, with $|d_3| \ll 1$. For the gold-plated combinations, the dependence on the light sea-quark mass is also weak, much weaker within our range of parameters than the dependence on a. Only for B_K does the variation with L_P have a similar magnitude to that with a. The values of the a^2 coefficient, d_4, indicate that scale describing a^2 effects ranges from ~ 0.3 GeV ($|d_4| \sim 1$) up to ~ 0.55 GeV ($|d_4| \sim 3.5$). These scales are not unusual for discretization errors with improved staggered fermions. The χ^2/d.o.f. of these fits is reasonable for B_K, G_{21}, and G_{24}.[4] Hence, we choose the results from the $\tilde{F}_1$ fits for

our central values for these quantities. However, we cannot use the $\tilde{F}_1$ results for G_{23} and G_{45}, since the fit quality is too poor. This is primarily due to the difficulty that the fits have in reproducing the dependence on a.

To obtain reasonable fits for G_{23} and G_{45}, we add higher order terms to the fitting function, denoting the new form $\tilde{F}_4$:

$$\tilde{F}_4 = \tilde{F}_1 + d_5(a\Lambda_Q)^2 \frac{L_P}{\Lambda_\chi^2} + d_6(a\Lambda_Q)^2 \left[\frac{S_P - m_{s\bar{s}}^2}{\Lambda_\chi^2}\right]$$
$$+ d_7(a\Lambda_Q)^2\alpha_s + d_8\alpha_s^2 + d_9(a\Lambda_Q)^4 \qquad (19)$$

where $\alpha_s = \alpha_s^{\overline{\text{MS}}}(1/a)$. In other words, we add a subset of the analytic terms quadratic in L_P, S_P and a^2, as well as two terms that include logarithmic dependence on a. The d_7 term would be the dominant source of a dependence were the action and operators tree-level $\mathcal{O}(a^2)$ improved. In fact, our valence fermion action and operators are not tree-level improved, so we must include the pure a^2 d_4 term as well. Nevertheless, we expect the tree-level contributions proportional to a^2 alone to be small, due to the use of HYP-smeared gauge fields. The d_8 term arises because our lattice operators are only matched to the continuum operators at one-loop order, leaving a two-loop residual discrepancy. In the $\tilde{F}_4$ fits we constrain d_{2-9} using the Bayesian method, choosing the prior conditions $d_{2-9} = 0 \pm 2$. Again we find that broadening the priors does not significantly improve the fits.

The results for the $\tilde{F}_4$ fits are shown (for $\mu = 2\,\text{GeV}$) in Table VIII and Figs. 7(b), 8(b), 9(b), 10(b), and 11(b). With the additional terms, we obtain reasonable values of χ^2/d.o.f for G_{23} and G_{45}, and we take the resulting extrapolated values as our final results for these two quantities. For the other quantities, the fit quality is only slightly improved.

As is apparent, particularly from Figs. 9(b), 10(b) and 11(b), the change from $\tilde{F}_1$ to $\tilde{F}_4$ fits has a very significant impact on the continuum extrapolation. This is primarily due to the $d_8\alpha_S^2$ term, which has a rapid dependence on a as $a \to 0$. We note that the coefficients of this term in the fits to G_{23} and G_{45} are relatively large [although still of $\mathcal{O}(1)$], and this is what leads to the large change in the extrapolated value between the fits. We do not find the $\tilde{F}_4$ fits to provide a convincing description of the a dependence, particularly as they depend very strongly on the result from the single ultrafine lattice. However, we think that the conservative choice is to use the better fit for the central value, and then to take the difference between the two fits as an estimate of the systematic error in the continuum-chiral extrapolation. The final results from the two fits, and the resulting estimate of the systematic error, are collected in Table IX. For G_{23}, G_{24} and G_{45} this source of error dominates all others, as discussed in the following section.

We have also used fit functions with additional higher-order terms. These do lead to mild reductions in the values of χ^2/d.o.f, but do not lead to significant changes

---

[4] Here we consider a value up to ~ 1.5 to be reasonable, due to residual correlations between configurations. We work with a bin size of 5, and Fig. 3 shows that this can lead to an underestimate of the error by $\sim 25\%$ on some configurations. Consequently the χ^2 will be overestimated by $\sim 1.25^2$.

TABLE VII. Results of $\tilde{F}_1$ fits to B_K and the gold-plated combinations. The renormalization scale is $\mu = 2\,\mathrm{GeV}$.

	B_K	G_{21}	G_{23}	G_{24}	G_{45}
d_1	0.5390(37)	1.0568(62)	1.4248(10)	0.5590(15)	1.2567(8)
d_2	-0.127(14)	0.095(27)	0.0275(33)	-0.0097(56)	0.0041(26)
d_3	0.006(15)	-0.014(25)	0.0145(30)	-0.0207(53)	0.0026(25)
d_4	0.78(25)	-1.92(41)	-1.799(64)	3.21(10)	-3.529(53)
B_K or G_i	0.5366(36)	1.0585(59)	1.4253(10)	0.5589(15)	1.2568(8)
χ^2/dof	1.53	1.30	2.01	1.08	4.07

(a) $\tilde{F}_1$: $\chi^2/\mathrm{d.o.f} = 1.53$ (b) $\tilde{F}_4$: $\chi^2/\mathrm{d.o.f} = 1.52$
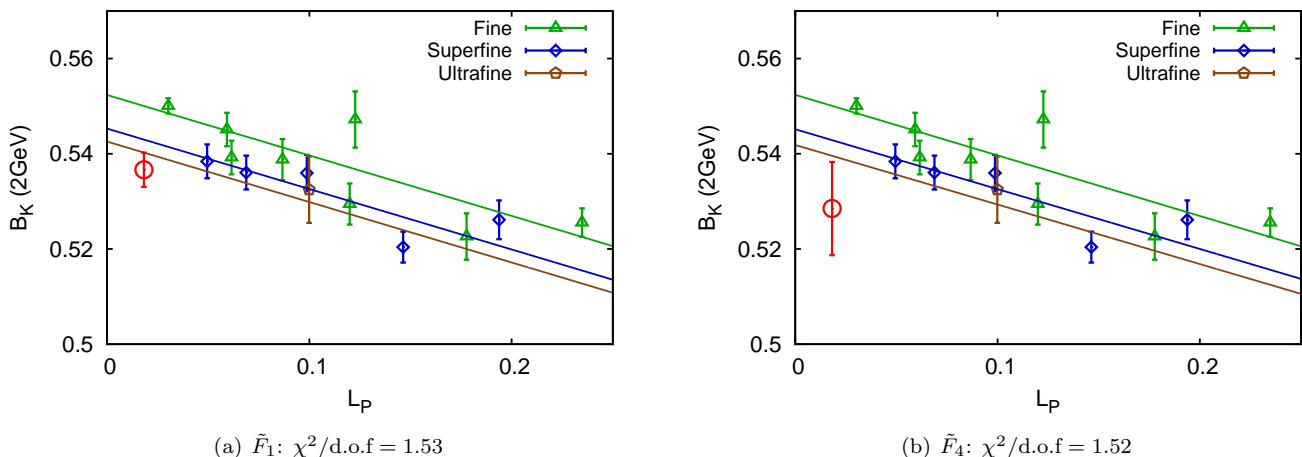
FIG. 7. Continuum-chiral extrapolation for B_K renormalized at $\mu = 2\,\mathrm{GeV}$. Results from the fine, superfine and ultrafine lattices are shown with (green) triangles, (blue) diamonds and the (brown) pentagon, respectively. (a) $\tilde{F}_1$ fit; (b) $\tilde{F}_4$ fit. The (red) circle gives the extrapolated result. Due to the variations in values of S_P and a, the curves should not pass precisely through all the points. For more discussion, see text.

in the central values compared to the $\tilde{F}_4$ fits. Thus they do not significantly change our estimates of systematic errors. For the sake of brevity, we do not display the results of these more elaborate fits.

We close this section by returning to the option of directly fitting the BSM B-parameters rather than using the gold-plated combinations. In all cases we find that direct continuum-chiral fits have values of $\chi^2/\mathrm{d.o.f.}$ in the range $3 - 5$, both for $\tilde{F}_1$ and $\tilde{F}_4$ (and more elaborate) fits. We do not fully understand this failure of the continuum-chiral fits, but suspect that it is related to errors in valence chiral extrapolation (X fits). The X fits are better controlled with the gold-plated combinations.

VI. FINAL RESULTS AND ERROR BUDGET

In this section we discuss all sources of error, and give our final results for the BSM B-parameters with their error budget. Because we obtain B_{2-5}^G using Eq. (6), we estimate the errors in B_K and the G_i first, and then propagate the errors to B_{2-5}^G. Our final results for the two standard renormalization scales are given in Tables X and

XI, while the final error budget is given in Table XII. [5]

As can be seen from Table XII, the statistical errors in B_K and the G_i are small, ranging from $\sim 0.25\%$ to $\sim 1\%$. The largest are those in G_{23} and G_{45}, resulting from the use of the $\tilde{F}_4$ fits for the continuum-chiral extrapolation. We propagate the statistical errors into the B_j^G using the bootstrap method. The larger errors in G_{23} and G_{45} then lead to B_3^G and B_5^G having the largest statistical errors of the BSM B-parameters. In all cases, however, the statistical errors are much smaller than those from systematic effects.

We now run through the systematic errors in the order listed in Table XII. The dominant error is that due to the combined effect of using one-loop matching and the continuum-chiral extrapolation. We combine these because the $\tilde{F}_4$ fit includes the α_s^2 error that results from perturbative truncation, and indeed this is the dominant contribution to the systematic error estimate, as

---

[5] The result quoted here for $B_K(2\,\mathrm{GeV})$ is obtained by a very slightly different analysis method than that we used previously in Ref. [9]. Thus the results differ slightly, although they agree within the (small) statistical errors, and have almost exactly the same total error.
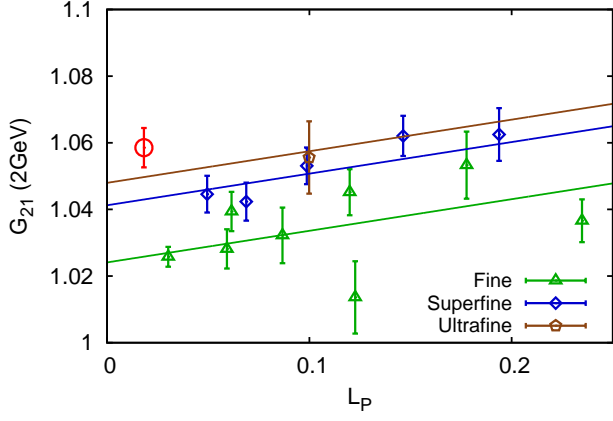
(a) $\tilde{F}_1$: $\chi^2/\text{d.o.f} = 1.30$
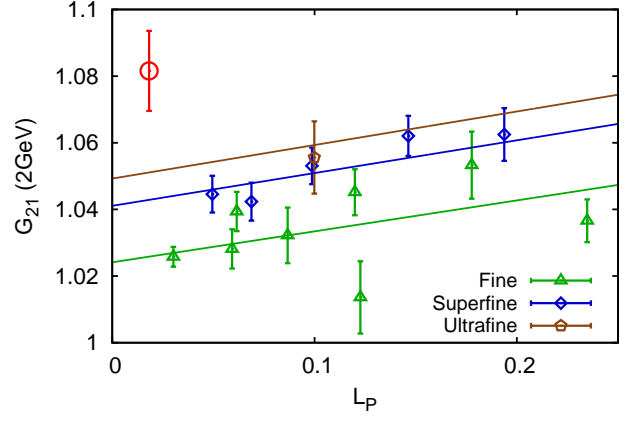
(b) $\tilde{F}_4$: $\chi^2/\text{d.o.f} = 1.23$

FIG. 8.   Continuum-chiral extrapolation results for G_{21} at $\mu = 2\,\text{GeV}$. The notation is as in Fig. 7.
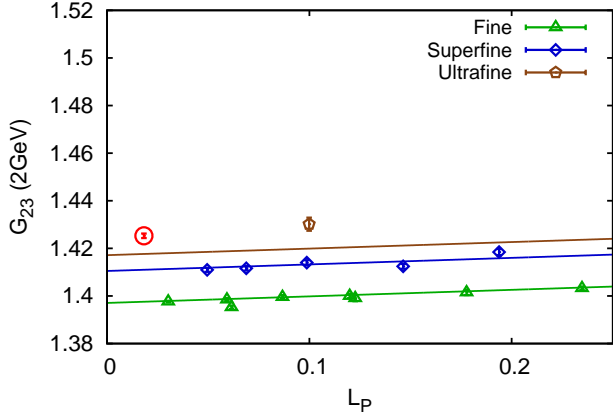
(a) $\tilde{F}_1$: $\chi^2/\text{d.o.f} = 2.01$
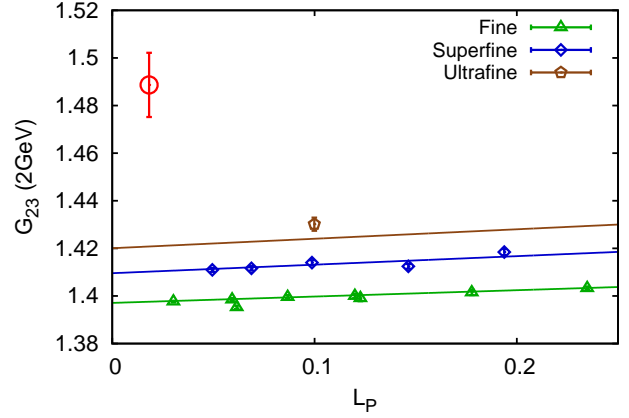
(b) $\tilde{F}_4$: $\chi^2/\text{d.o.f} = 1.33$

FIG. 9.   Continuum-chiral extrapolation results for G_{23} at $\mu = 2\,\text{GeV}$. The notation is as in Fig. 7.
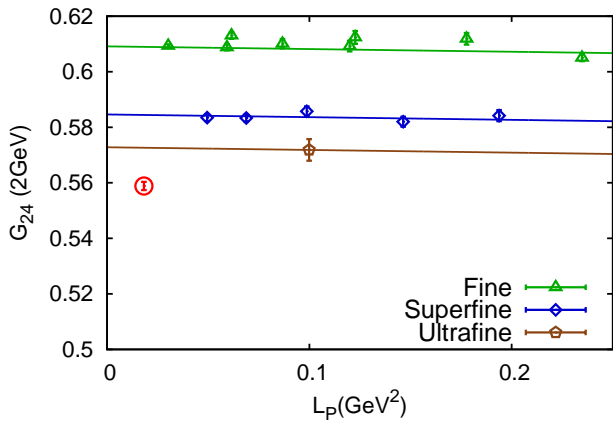
(a) $\tilde{F}_1$: $\chi^2/\text{d.o.f} = 1.08$
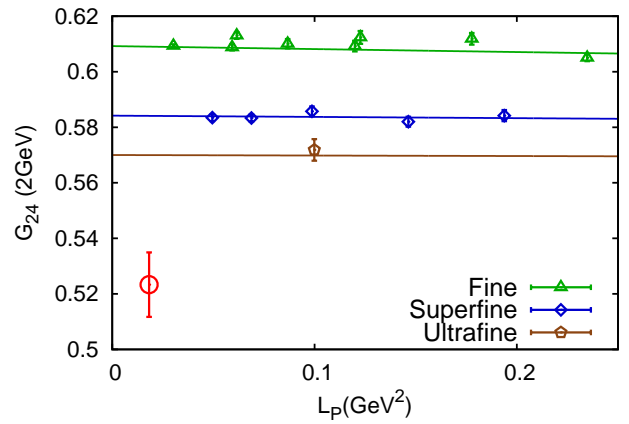
(b) $\tilde{F}_4$: $\chi^2/\text{d.o.f} = 0.91$

FIG. 10.   Continuum-chiral extrapolation results for G_{24} at $\mu = 2\,\text{GeV}$. The notation is as in Fig. 7.
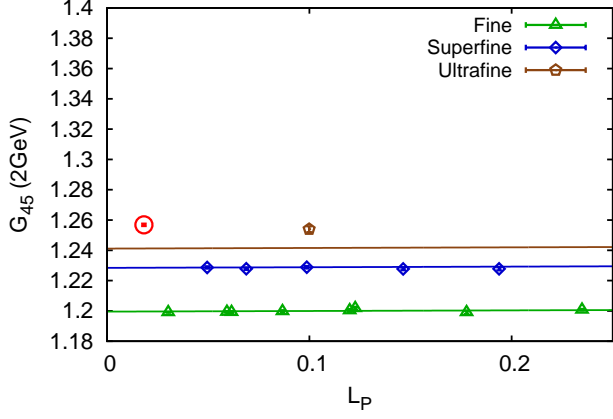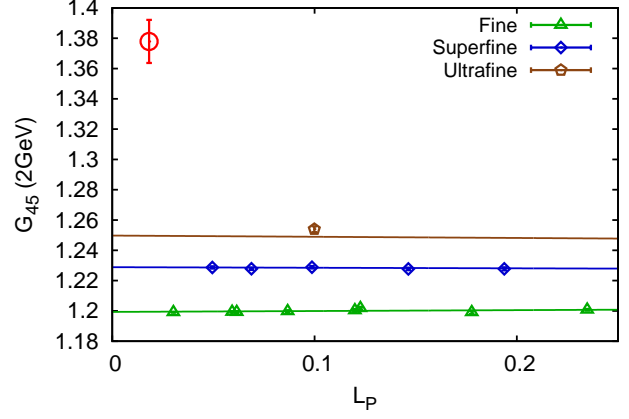
(a) $\tilde{F}_1$: $\chi^2/\text{d.o.f} = 4.07$ (b) $\tilde{F}_4$: $\chi^2/\text{d.o.f} = 1.39$

FIG. 11. Continuum-chiral extrapolation results for G_{45} at $\mu = 2\,\text{GeV}$. The notation is as in Fig. 7.

TABLE VIII. Fit results for BSM B-parameters and the gold-plated combinations obtained using $\tilde{F}_4$-fit at $\mu = 2\,\text{GeV}$.

	B_K	G_{21}	G_{23}	G_{24}	G_{45}
d_1	0.5308(99)	1.080(12)	1.488(14)	0.523(12)	1.378(14)
d_2	-0.124(18)	0.104(28)	0.045(14)	0.001(16)	-0.013(12)
d_3	0.005(15)	-0.011(25)	0.019(6)	-0.021(6)	0.012(7)
d_4	0.24(40)	-0.33(27)	2.22(75)	0.84(63)	3.70(80)
d_5	-0.18(77)	-0.66(48)	-1.10(87)	-0.7(10)	1.16(78)
d_6	0.10(10)	-0.081(63)	-0.29(34)	0.03(22)	-0.64(42)
d_7	0.09(21)	-0.10(14)	1.20(40)	0.33(33)	2.06(42)
d_8	0.22(21)	-0.65(20)	-1.80(37)	0.98(31)	-3.34(39)
d_9	0.008(31)	-0.008(21)	0.183(60)	0.036(50)	0.322(64)
B_K or G_i	0.5285(98)	1.082(12)	1.489(13)	0.523(12)	1.378(14)
χ^2/dof	1.52	1.23	1.33	0.91	1.39

TABLE IX. Results for B_K and G_i (renormalized at $\mu = 2\,\text{GeV}$) from continuum-chiral extrapolation using the $\tilde{F}_1$ and $\tilde{F}_4$ fits. Our choices for the final central values are (red and) underlined. Δ is the fractional systematic error in the continuum-chiral extrapolation, and is obtained from the difference between the two fits.

	$\tilde{F}_1$	$\tilde{F}_4$	$\Delta(\%)$
B_K	0.5366(36)	0.5285(98)	1.52
G_{21}	1.0585(59)	1.082(12)	2.18
G_{23}	1.4253(10)	1.489(13)	4.26
G_{24}	0.5589(15)	0.523(12)	6.36
G_{45}	1.2568(8)	1.378(14)	8.79

TABLE X. Final results for B_K and the BSM B-parameters at renormalization scales $\mu = 2\,\text{GeV}$ and $\mu = 3\,\text{GeV}$. The first error is statistical, the second systematic.

	$\mu = 2\,\text{GeV}$	$\mu = 3\,\text{GeV}$
B_K	0.537(4)(26)	0.519(4)(26)
B_2^G	0.568(1)(25)	0.525(1)(23)
B_3^G	0.382(4)(17)	0.360(4)(16)
B_4^G	0.984(3)(64)	0.981(3)(62)
B_5^G	0.714(7)(71)	0.751(7)(68)

discussed above. However, one can also estimate the truncation error directly, following Ref. [8], by the size of a typical two-loop contribution:

$$\Delta B_i \approx B_i \times \alpha_s^2. \tag{20}$$

Here we use α_s in the $\overline{\text{MS}}$ scheme evaluated at a scale $1/a_{\min}$, where $a_{\min}$ is our smallest lattice spacing. This leads to a 4.4% relative error. To avoid double-counting, we take the larger of (a) the direct estimate of two-loop effects (4.4%) and (b) the difference between $\tilde{F}_1$ and $\tilde{F}_4$ fits. In essence this method is using the $\tilde{F}_4$ fit to give an estimate of the uncertainty in the coefficient of the α_s^2 term, except that we do not allow this uncertainty to drop below unity.

The above description applies to quantities we calculate directly, namely B_K and the G_i. For the derived quantities B_j^G, defined in Eq. (6), we proceed as follows. We vary the fit choices (for the continuum-chiral extrapolation) for each of the components of the B_j^G independently, and take the largest variation from the central value as the systematic error estimate. If this maximum

TABLE XI. Final results for the gold-plated combinations G_i. Notation as in Table X.

	$\mu = 2\,\text{GeV}$	$\mu = 3\,\text{GeV}$
G_{21}	1.059(6)(52)	1.012(6)(50)
G_{23}	1.489(13)(66)	1.460(14)(65)
G_{24}	0.559(1)(36)	0.515(1)(32)
G_{45}	1.378(14)(123)	1.307(14)(107)

value lies below 4.4%, we replace the estimate with the direct two-loop estimate of a 4.4% error.

We next consider the error due to the finite volume (FV) of the lattice. We estimate this from the difference between results on the C3 and C3-2 ensembles, which differ only in their spatial volumes. This is not entirely satisfactory, since we do not use coarse lattices in our final continuum-chiral extrapolation. However, we stress that the dominant FV error, as estimated by SChPT, comes from valence pions propagating to adjacent periodic volumes. This is because the arguments of the chiral logarithms of Eq. (10) are the squared masses of valence pions, X_B. Since on each ensemble we are extrapolating to the physical valence quark masses, the dominant FV effects are present, even though on ensembles C3 and C3-2 we are far from the physical values of L_P and a. In our calculation of B_K, we have used the comparison of doing the X-fits with finite- and infinite-volume SChPT forms as an alternative estimate of the FV error [40]. However, this method is not useful for the gold-plated combinations, since they do not contain NLO chiral logarithms.

Our method of estimating systematic errors arising from the X fits has been described in Sec. IV. We repeat the entire analysis using different priors for the X-fits, and using the ES method. Each leads to a change in the final values of the quantities of interest. We combine the fractional shifts in quadrature to obtain our total systematic error.

Our method of estimating the systematic error arising from Y fits, as noted above, is to repeat the entire analysis (including the continuum-chiral extrapolation) using quadratic, as apposed to linear, functional forms. This differs slightly from the estimate we used in Ref. [9], where we used the shift in the quantities on a specific MILC ensemble. The Y fit errors turn out to be of comparable size to those from X fits, ranging up to 2%.

The remaining two systematic errors are very small, and have essentially no impact on the total error. We include them for completeness. The first concerns the value of the pion decay constant f that we use in the chiral logarithms of Eq. (10). At NLO we could equally well use the physical value $f_\pi = 130.41\,\text{MeV}$ [41] or the value in the chiral limit, $f_\pi \approx 124.2\,\text{MeV}$ [32]. In practice we use $f = 132\,\text{MeV}$ (close to the physical value) for our central value, and repeat the entire analysis using $f = 124.2\,\text{MeV}$ (the chiral-limit value) to estimate the systematic error. In fact, only B_K is sensitive to this choice, since the gold-plated combinations contain no NLO chiral logarithms. Thus the 0.1% error that results in B_K propagates unchanged into all of the BSM B-parameters.

Finally, the parameter we use to set the scale, r_1, has an error which propagates into all the final results. To estimate this, we repeat the entire analysis with the central value for r_1 replaced by $r_1 \pm \sigma_{r_1}$, and quote the maximum difference in each quantity as the systematic error. The resulting errors are very small ($\sim 0.1 - 0.35\%$), reflecting the fact that the B-parameters are dimensionless.

TABLE XII. Error budget for the B_i and G_j evaluated at renormalization scale $\mu = 2\,\mathrm{GeV}$. All entries are in percent.

cause	B_K	G_{21}	G_{23}	G_{24}	G_{45}	B_2^G	B_3^G	B_4^G	B_5^G	$B_3^{G,\mathrm{SUSY}}$	method
statistics	0.67	0.56	0.87	0.27	1.02	0.25	1.00	0.27	0.98	0.66	see text
$\left\{\begin{array}{l}\text{matching}\\\text{cont-extrap.}\end{array}\right\}$	4.40	4.40	4.40	6.36	8.79	4.40	4.45	6.36	9.63	4.40	($\tilde{F}_1$ vs. $\tilde{F}_4$) or α_s^2 (U1)
finite volume	0.73	0.17	0.05	0.43	0.04	0.56	0.52	0.99	1.02	0.60	(C3) vs. (C3-2)
X-fits	0.05	0.40	0.45	0.02	0.96	0.36	0.34	0.37	1.23	0.60	change Bayes. prior & fit method
Y-fits	2.07	2.11	0.32	0.48	1.12	0.00	0.32	0.48	1.59	0.22	linear vs. quad.
f_π	0.10	0	0	0	0	0.10	0.10	0.10	0.10	0.10	132 MeV vs. 124.2 MeV.
r_1	0.35	0.28	0.11	0.16	0.21	0.07	0.17	0.09	0.30	0.01	errors due to r_1 ambiguity.
Total	4.93	4.91	4.44	6.39	8.92	4.45	4.51	6.47	9.90	4.49	

VII. COMPARISONS AND OUTLOOK

In Table XIII and Fig. 12 we compare our results for the B-parameters to those from other collaborations. This is done at $\mu = 3\,\mathrm{GeV}$ since results from all collaborations are available at this choice of renormalization scale. The RBC-UKQCD collaboration uses $N_f = 2 + 1$ light flavors of domain wall quarks, and NPR for the matching between lattice and continuum theories. In 2012, RBC-UKQCD used the RI-MOM scheme for this matching [21], while the preliminary 2015 results are obtained using several RI-SMOM schemes, in the spirit of Ref. [27]. Both schemes are connected to the $\overline{\mathrm{MS}}$ scheme using one-loop perturbation theory. The ETM collaboration uses twisted-mass Wilson quarks. The original results from 2012 were with $N_f = 2$ light sea quarks and a quenched valence strange quark [13], while the 2015 results are from an $N_f = 2 + 1 + 1$ simulation including both strange and charmed sea quarks [3]. Both ETM calculations match lattice and continuum operators using NPR in the RI-MOM scheme.

Both RBC-UKQCD and ETM results are quoted using the so-called SUSY basis of BSM four-fermion operators [42]. The only BSM B-parameter which differs from that in the basis of Buras et al. (Ref. [31]) that we use is B_3,

$$B_3^{\mathrm{SUSY}} = -\frac{3}{2}B_3^{\mathrm{Buras}} + \frac{5}{2}B_2^{\mathrm{Buras}}. \qquad (21)$$

We use this equation to determine our result for B_3^{SUSY} quoted in Table XIII.

For completeness, we note that our 2013 results for the BSM B-parameters (Ref. [23]) are superseded and corrected by our present results.[6] We now have significantly more ensembles, allowing a better controlled continuum-chiral extrapolation. This addition required us to change from $\tilde{F}_1$ fits to $\tilde{F}_4$ fits for G_{23} and G_{45}, which, as shown above, significantly changes the central values for these quantities. In addition, we found an error in our RG running due to the use of an incorrect two-loop contribution to the pseudoscalar anomalous dimension [needed for the denominators of the BSM B-parameters—see Eq. (3)]. Correcting this error leads to $\sim 5\%$ reductions in all the BSM B-parameters. A detailed description of the effect of these changes is given in Ref. [24]. The overall effect is that our new results for B_2, B_3^{SUSY}, B_4 and B_5 are reduced by about 5%, 3%, 5% and 12%, respectively, compared to those in Ref. [23].

Table XIII shows that the results for B_K, B_2 and B_3^{SUSY} are consistent across all calculations, with all results having comparable errors. By contrast, there are significant differences for B_4 and B_5, as one can see most clearly from Fig. 12. The preliminary results from RBC-UKQCD (2015) using the intermediate RI-SMOM schemes are consistent with our results, while those using the intermediate RI-MOM scheme [RBC-UK (2012), ETM (2012) and ETM (2015)] differ significantly. For example, the ETM (2015) results for B_4 and B_5 differ from our results by 2.6σ and 3.2σ, respectively.

The pattern of results in the Table suggests that the ultimate source of these differences may well be the matching from lattice matrix elements to those in the continuum $\overline{\mathrm{MS}}$ scheme. In our calculation, this error is due to the truncation of matching factors at one-loop order. For B_4 and B_5 (the two B-parameters which differ from the results obtained using the RI-MOM scheme) our error estimate is taken as the difference between fits using $\tilde{F}_1$ and $\tilde{F}_4$ fit forms (see Figs. 10 and 11). While we consider this to be a conservative estimate, we cannot rule out that it is an underestimate due to unexpectedly large α^2 terms in the matching factors. In the case of the calculations using the NPR method, the significant differences between results obtained using RI-MOM and RI-SMOM schemes indicate an underestimate of the associated systematic errors. This could be a problem specifically related to the RI-MOM scheme, where one must subtract unwanted contributions from pion poles, a source of systematic errors absent in the RI-SMOM schemes [43]. Or it could be due to large truncation errors in the relation between one or both of these schemes and the $\overline{\mathrm{MS}}$ scheme.

Clearly these issues require further investigation. One possibility is for all the calculations to use the same intermediate scheme such as RI-SMOM and then to di-

---

[6] This does not apply to B_K, for which our present result is essentially the same as that from Ref. [23].

TABLE XIII. Comparison of the BSM B-parameters at renormalization scale $\mu = 3\,\mathrm{GeV}$ obtained using different fermion discretizations. The RBC-UKQCD results using domain-wall fermions are RBC-UK (2012) [21] and the preliminary results (with incomplete error budget) of RBC-UK (2015) [25]. The ETM collaboration results using twisted-mass fermions are ETM (2012) [13] and ETM (2015) [3]. N.A. means "not available".

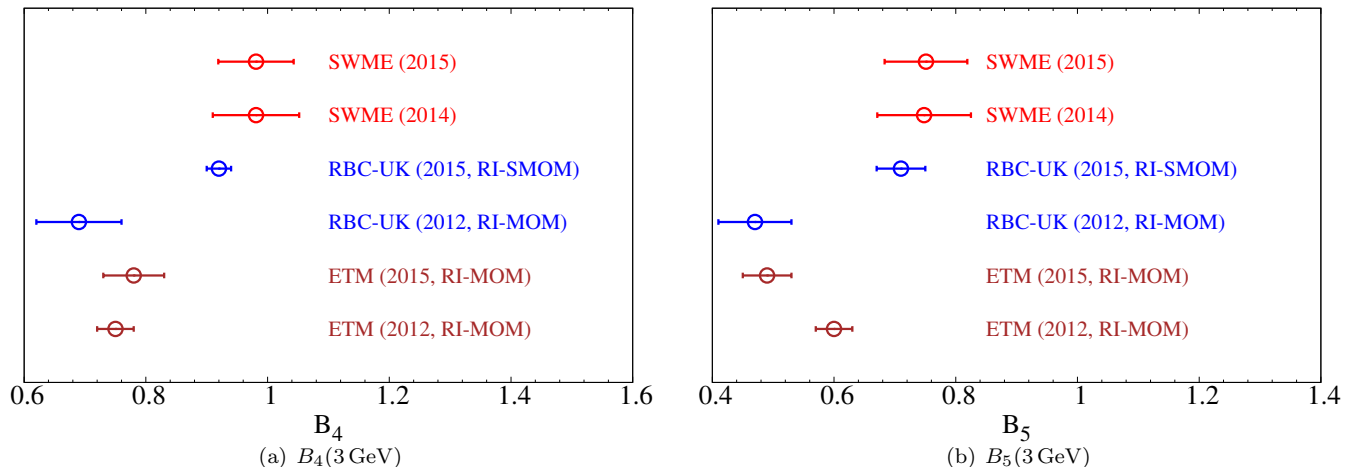|	SWME (this work)	RBC-UK (2012)	RBC-UK (2015)	ETM (2012)	ETM (2015)
B_K	0.519(4)(26)	0.53(2)	0.53(1)	0.51(2)	0.51(2)
B_2	0.525(1)(23)	0.43(5)	0.49(2)	0.47(2)	0.46(3)
B_3^{SUSY}	0.773(6)(35)	0.75(9)	0.74(7)	0.78(4)	0.79(5)
B_3^{Buras}	0.360(4)(16)	N.A.	N.A.	N.A.	N.A.
B_4	0.981(3)(62)	0.69(7)	0.92(2)	0.75(3)	0.78(5)
B_5	0.751(7)(68)	0.47(6)	0.71(4)	0.60(3)	0.49(4)

(a) $B_4(3\,\mathrm{GeV})$

(b) $B_5(3\,\mathrm{GeV})$

FIG. 12. Comparison of results for B_4 and B_5 at $\mu = 3\,\mathrm{GeV}$. The references for the points are, proceeding from top to bottom, this work (SWME 2015), [24] (SWME 2014), [25] (RBC-UK 2015), [21] (RBC-UK 2012), [3] (ETM 2015) and [13] (ETM 2012).

rectly compare results in that scheme. This reduces the dependence on perturbation theory as one does not need to to match to the $\overline{\mathrm{MS}}$ scheme. One would still need to evolve between different scales in the RI-SMOM scheme, but this could also, ultimately, be done non-perturbatively [44]. To these ends we are pursuing the implementation of NPR using staggered fermions [45–47].

[1] S. Aoki *et al.*, Eur. Phys. J. **C74**, 2890 (2014), arXiv:1310.8555 [hep-lat].

[2] T. Blum *et al.* (RBC, UKQCD), (2014), arXiv:1411.7017 [hep-lat].

[3] N. Carrasco *et al.* (ETM), (2015), arXiv:1505.06639 [hep-lat].

[4] S. Durr *et al.*, Phys. Lett. **B705**, 477 (2011), arXiv:1106.3230 [hep-lat].

[5] C. Aubin, J. Laiho, and R. S. Van de Water, Phys.Rev. **D81**, 014507 (2010), arXiv:0905.3947 [hep-lat].

[6] J. Laiho and R. S. Van de Water, PoS **LATTICE2011**, 293 (2011), arXiv:1112.4861 [hep-lat].

[7] T. Bae, Y.-C. Jang, C. Jung, H.-J. Kim, J. Kim, *et al.*, Phys.Rev. **D82**, 114509 (2010), arXiv:1008.5179 [hep-lat].

[8] T. Bae, Y.-C. Jang, C. Jung, H.-J. Kim, J. Kim, J. Kim, K. Kim, S. Kim, W. Lee, S. R. Sharpe, and B. Yoon, Phys.Rev.Lett. **109**, 041601 (2012), arXiv:1111.5698 [hep-lat].

[9] T. Bae *et al.* (SWME), Phys.Rev. **D89**, 074504 (2014), arXiv:1402.0048 [hep-lat].

[10] J. A. Bailey, Y.-C. Jang, W. Lee, and S. Park (SWME), Phys. Rev. **D92**, 034510 (2015), arXiv:1503.05388 [hep-lat].

[11] J. Laiho, E. Lunghi, and R. S. Van de Water, Phys.Rev. **D81**, 034503 (2010), arXiv:0910.2928 [hep-ph].

[12] Z. Bai, N. H. Christ, T. Izubuchi, C. T. Sachrajda, A. Soni, and J. Yu, Phys. Rev. Lett. **113**, 112003 (2014), arXiv:1406.0916 [hep-lat].

[13] V. Bertone *et al.* (Collaboration ETM), JHEP **1303**, 089 (2013), arXiv:1207.1287 [hep-lat].

[14] M. Ciuchini, V. Lubicz, L. Conti, A. Vladikas, A. Donini, *et al.*, JHEP **9810**, 008 (1998), arXiv:hep-ph/9808328 [hep-ph].

[15] M. Bona *et al.* (UTfit Collaboration), JHEP **0603**, 080 (2006), arXiv:hep-ph/0509219 [hep-ph].

[16] G. Isidori, Y. Nir, and G. Perez, Ann.Rev.Nucl.Part.Sci. **60**, 355 (2010), arXiv:1002.0900 [hep-ph].

[17] M. Blanke, A. J. Buras, K. Gemmler, and T. Heidsieck, JHEP **1203**, 024 (2012), arXiv:1111.5014 [hep-ph].

[18] C. R. Allton, L. Conti, A. Donini, V. Gimenez, L. Giusti, G. Martinelli, M. Talevi, and A. Vladikas, Phys. Lett. **B453**, 30 (1999), arXiv:hep-lat/9806016 [hep-lat].

[19] A. Donini, V. Gimenez, L. Giusti, and G. Martinelli, Phys. Lett. **B470**, 233 (1999), arXiv:hep-lat/9910017 [hep-lat].

[20] R. Babich, N. Garron, C. Hoelbling, J. Howard, L. Lellouch, and C. Rebbi, Phys. Rev. **D74**, 073009 (2006), arXiv:hep-lat/0605016 [hep-lat].

[21] P. Boyle, N. Garron, and R. Hudspith (RBC Collaboration, UKQCD Collaboration), Phys.Rev. **D86**, 054028 (2012), arXiv:1206.5737 [hep-lat].

[22] G. Martinelli, C. Pittori, C. T. Sachrajda, M. Testa, and A. Vladikas, Nucl. Phys. **B445**, 81 (1995), arXiv:hep-lat/9411010 [hep-lat].

[23] T. Bae *et al.* (SWME), Phys. Rev. **D88**, 071503 (2013), arXiv:1309.2040 [hep-lat].

[24] J. Leem *et al.* (SWME), PoS **LATTICE2014**, 370 (2014), arXiv:1411.1501 [hep-lat].

[25] R. J. Hudspith, N. Garron, and A. T. Lytle (2015) arXiv:1512.05398 [hep-lat].

[26] RBC-UKQCD Collaboration, in preparation (2015).

[27] C. Sturm, Y. Aoki, N. H. Christ, T. Izubuchi, C. T. C. Sachrajda, and A. Soni, Phys. Rev. **D80**, 014501 (2009), arXiv:0901.2599 [hep-ph].

[28] J. A. Bailey, H.-J. Kim, W. Lee, and S. R. Sharpe, Phys.Rev. **D85**, 074507 (2012), arXiv:1202.1570 [hep-lat].

[29] J. Kim, W. Lee, and S. R. Sharpe, Phys. Rev. **D83**, 094503 (2011), arXiv:1102.1774 [hep-lat].

[30] J. Kim, W. Lee, J. Leem, S. R. Sharpe, and B. Yoon (SWME), Phys.Rev. **D90**, 014504 (2014), arXiv:1404.2368 [hep-lat].

[31] A. J. Buras, M. Misiak, and J. Urban, Nucl.Phys. **B586**, 397 (2000), arXiv:hep-ph/0005183 [hep-ph].

[32] A. Bazavov, D. Toussaint, C. Bernard, J. Laiho, C. DeTar, *et al.*, Rev.Mod.Phys. **82**, 1349 (2010), arXiv:0903.3598 [hep-lat].

[33] C. Bernard (MILC Collaboration), private communication (2012).

[34] J. A. Bailey, A. Bazavov, C. Bernard, C. Bouchard, C. DeTar, *et al.*, Phys.Rev. **D85**, 114502 (2012), arXiv:1202.6346 [hep-lat].

[35] A. Hasenfratz and F. Knechtli, Phys.Rev. **D64**, 034504 (2001), arXiv:hep-lat/0103029 [hep-lat].

[36] W.-j. Lee and S. R. Sharpe, Phys.Rev. **D66**, 114501 (2002), arXiv:hep-lat/0208018 [hep-lat].

[37] C. Davies, E. Follana, I. Kendall, G. P. Lepage, and C. McNeile (HPQCD Collaboration), Phys.Rev. **D81**, 034506 (2010), arXiv:0910.1229 [hep-lat].

[38] B. Yoon, Y.-C. Jang, C. Jung, and W. Lee, J. Korean Phys. Soc. **63**, 145 (2013), arXiv:1101.2248 [hep-lat].

[39] G. P. Lepage *et al.*, Nucl. Phys. Proc. Suppl. **106**, 12 (2002), arXiv:hep-lat/0110175.

[40] J. Kim, C. Jung, H.-J. Kim, W. Lee, and S. R. Sharpe, Phys.Rev. **D83**, 117501 (2011), arXiv:1101.2685 [hep-lat].

[41] J. Beringer *et al.* (Particle Data Group), Phys.Rev. **D86**, 010001 (2012).

[42] F. Gabbiani, E. Gabrielli, A. Masiero, and L. Silvestrini, Nucl.Phys. **B477**, 321 (1996), arXiv:hep-ph/9604387 [hep-ph].

[43] A. T. Lytle, P. A. Boyle, N. Garron, R. J. Hudspith, and C. T. Sachrajda (RBC-UKQCD), (2013), arXiv:1311.0322 [hep-lat].

[44] R. Arthur and P. A. Boyle (RBC, UKQCD), Phys. Rev. **D83**, 114511 (2011), arXiv:1006.0422 [hep-lat].

[45] A. T. Lytle and S. R. Sharpe, Phys. Rev. **D88**, 054506 (2013), arXiv:1306.3881 [hep-lat].

[46] J. Kim, J. Kim, W. Lee, and B. Yoon, PoS **LATTICE2013**, 308 (2014), arXiv:1310.4269 [hep-lat].

[47] H. Jeong, J. Kim, J. Kim, W. Lee, J. Pak, and S. Park (SWME), PoS **LATTICE2014**, 286 (2015), arXiv:1410.6607 [hep-lat].